The authors greatly appreciate the constructive comments from the reviewer #1.
The reviewer maintains that the manuscript demonstrates the importance of mixing states of dust and BC particles on their optical properties. The reviewer underlines that the topic is important to the atmospheric science community, although further understanding of the abundance of mineral dust particles with black carbon in the atmosphere is needed, as the authors also emphasize in the manuscript.

We revised our manuscript with a number of changes in response to the reviewer's comments. The specifics are listed below.

Rev. 1: General comments: **I suggest having a brief discussion regarding why and how optical properties of mineral dust mixed with black carbon differ from those of bare mineral dust/black carbon. I assume that microphysical configuration such as lens effect (Bond et al., 2006) and shadowing of mineral dust particles to black carbon may contribute to the optical properties of mineral dust/black carbon mixed particles. This discussion will be useful to have a general conclusion since this paper discuss a limited number of modeled particles. Example is Page 2504 Line 27-28: While DDSCAT predicts for internally mixed particles larger than 500nm (BL2S3–BL2S5) an increase of SSA at all wavelengths compared to bare dust particles (S3–S4–S5). Please discuss the reason.**

Commenting on the *relevance of selected number of simulations* in a computational intensive spectral range.

The paper addresses how optical properties of polluted mineral dust aerosols might vary depending on the details of the mixing with black carbon particles and the mineral dust size. Internal mixtures of BC and dust have been found in many geographical locations. The strongest impact of polluted dust, discussed in literature, has been found in Asia, due to the high load of absorbing aerosols (black carbon, mineral dust and mixtures). It has been demonstrated that these aerosols have an impact on both the spatial and temporal distribution of high precipitation events. The simulations performed in our study *are computationally* intensive, due to the aerosol *sizes* and the (short) wavelengths selected. The spectral signature of the aerosol ensemble has been characterized in the UV-VIS-NIR, spectral range that has not been explored from other authors yet, despite the significance for remote sensing retrieval and climate modeling.

Commenting on the *effect of mixing on optical properties of BC and mineral dust*.

The configurations studied in this manuscript have been observationally constrained and *do not include embedding*. The *BC* particle is *laying on the surface of mineral dust*. So, there is no "traditional lens effect", where incident light is focused on the core of the particle. When simulating internal mixtures, the size of the BC aggregate is kept the same, while we increase the dust particle size. Regarding optical properties and differences between bare BC, mineral dust and internal mixtures:

1. Internal mixture vs. bare BC: With the increase in size of mineral dust increases absorption, but also largely the scattering of the internal mixture, leading to larger SSA values for internal mixtures compared to bare BC (in all cases BL2S1 – BL2S5). The increase in the absorption in the internal mixture compared to bare BC, despite no embedding (and therefore no lens effect, see also Scarnato et al., 2013) is due to absorption properties of mineral dust.
2. Internal mixture vs. bare mineral dust: Interestingly, when comparing the internal mixtures cases BL2S1 – BL2S5 with bare mineral dust optical properties, we found a "cut off" in the SSA values, depending on the size of the 2 internally mixed aerosols: 1. Simulations predict for small internally mixed particles (cases BL2S1 and BL2S2), where dust particles are small in size, a steep increase in the absorption and no significant variation in the scattering properties compared to bare

mineral dust. The latter leads to smaller SSA values of internal mixtures compared to bare mineral dust particles. 2. When mineral dust particles are larger and therefore the BC mass is comparably much smaller than the mass of mineral dust (cases BL2S3-BL2S5), simulations predict a steep increase in the scattering, but less in the absorption, therefore prevails scattering vs. absorption, leading to the larger SSA.

The authors added after the sentence "While DDSCAT predicts [ ]…. bare dust particles (S3-S4-S5)." the following text:

Such a "cut off" in SSA values is due to the fact that simulations predict for small internally mixed particles (cases BL2S1 and BL2S2), where dust particles are small in size, a steep increase in the absorption and no significant variation in the scattering properties compared to bare mineral dust (S1-S2). The latter leads to smaller SSA values of internal mixtures compared to bare mineral dust particles. Further, when mineral dust particles are large (cases S3-S5), and therefore the BC mass (case BL2) results comparatively much smaller than the mass of case S3 and S5), DDSCAT simulations predict a steep increase in the scattering, but less in the absorption, therefore prevailing scattering vs. absorption, for those cases are associated with larger SSA values compared to bare mineral dust.

In an attempt to synthesize the differences between the above discussed optical properties of bare BC and internal mixtures, we found that:
With the increase in size of mineral dust the absorption increases; however, also the scattering of the internal mixture (cases BL2S1 – BL2S5) increases leading to larger SSA values for internal mixtures compared to bare BC (case BL2) (not shown here, as we provide MAC normalized by the total mass of the particle, not just BC mass). The increase in the absorption, despite no embedding (no "lens effect"), see also Scarnato et al., 2013, is due to absorption properties of mineral dust.

Specific comments

1. **P2488L14-16 The meaning of "the opposites" is not clear here.**

We modified the sentence in the following way:

"Predicted values of mass absorption, scattering and extinction coefficients (MAC, MSC, MEC) for bare BC show a weak dependence on the BC aggregate size, while the asymmetry parameter (g) shows an opposite behavior."

1. **P2489 L18: Semicolon (;) may be comma.**

We modified the text adding a period.

2. **P2493 L9: Take out parenthesis.**

We removed the parenthesis, thanks for noticing.

3. **P2494: L4 and 7: Some words are italic. Is there any intention?**

We just wanted to underline that was just a minor aspect discussed in the paper.

4. **P2496 L7: In this study, we modeled dust aerosols as spheroids and rectangular prisms with an intermediate aspect ratio of 1.75. . . (see Table 3). The aspect ratio of 1.75 is not intermediate but the maximum value (Table 3).**

We modified the text for clarification in the following way:
"In this study, we modeled dust aerosols as spheroids and rectangular prisms with an intermediate aspect ratio (compared to the literature) of 1.75, ⋯ []"

5. **P2498 L18 For synthetic aggregates presented in Fig. 2, . . . I am not sure why the number of each particle has standard deviation (SD). Is this an averaged number? Please explain the meaning.**

Yes, they are averages. The number estimates is sensitive to orientation, therefore the SD is calculated from 50 random orientations.

6. **P2500 L27: Table 4 should be Table 5.**

Thanks for noticing it. We modified the text accordingly.

7. **Table 2: Table 2 is not useful unless the refractive indices values are shown. Also Wagner et al. (2012) showed a range of refractive index for mineral dust. Which values did the authors use?**

As the referee commented, Wagner et al. 2012 provided a range of values for Sahara dust. We used the upper range of values for the imaginary part of the mineral dust refractive indexes.

The comment of the referee on the utility of Table 2 is justified. Despite that, the choice to keep Table 2 is motived by the fact that, in this way, a quick reader does not have to scan all the paper to find the reference refractive indexes.

8. **Table 3: Please indicate how many particles were analyzed to obtain these values.**

The values in Table 3 provide morphological descriptors for the images shown in Fig. 1

9. **Figure 1: It will be useful to have arrows to indicate black carbon on the mineral dust particles.**

We modified the images adding red circles around the BC aggregates on the surface of the mineral dust particles.

The authors greatly appreciate the constructive comments from the reviewer #2. The reviewer maintains that the methodology described in the paper is a good and a reasonable strategy, already, introduce by Scarnato et al., 2013. The peculiarity of methodology combines particle shape observations to numerical simulations, and it is of relevance for both climate and remote sensing applications. The reviewer also recommended publication of the paper after considering the following suggestions and minor corrections. We revised our manuscript in a number of locations in response to the reviewer's comments. The specifics are listed below.

1. Because the subject is relevant for climate modelling and remote sensing, it would be convenient for readers working in these fields to compare the optical properties calculated here with such based on approximations commonly applied in climate models and inversion algorithms, e.g., to results from Mie calculations for spherical particles with volume equivalent radius.

We convene with the reviewer, that BC particles are typically assumed to be spherical in both climate models and (depending on the aerosol type) in remote sensing retrievals. The authors provided equivalent volume Mie-simulations for BC aggregates with similar characteristics in Scarnato ACP (2013) and China et al., (2015), so we added the references and modified the text in the following way:

"Large differences in both magnitude and spectral dependency are found in optical properties of BC aggregates compared to equivalent volume spherical particles, the biases and their relevance for radiative forcing estimates with different surface albedo are discussed in Scarnato et al., 2013 and China et al., 2015".

Dust particles morphology assumptions may vary in remote sensing retrieval algorithms. AERONET retrieval assumes dust particles to be spheroidal, while MISR retrieval (16+) uses spheroidal, grain, plate shapes. Our paper discusses a subset of those shapes, such as plates and spheroidal particles. The text has been modified in the following way:

"Both orbital and ground based remote sensing techniques use a pre-selected library of aerosol types in the analysis of radiometric data. The computations of optical properties for the library often make use of spherical shape assumptions.

The assumptions of mineral dust particles shape may vary in the retrieval algorithms. AERONET retrieval assumes mineral dust particles to be spheroidal (Dubovik et al, 2006), while MISR retrieval (version 16+) uses spheroidal, grain, plate and spherical shapes (Kalashnikova et al., 2013).
The retrieval algorithms select an aerosol type based on the best fit to radiance measurements [i.e.](Deuze et al., 2001, Hasekamp et al. 2011)."

2. Introduction, end of 1st paragraph: further studies considering core-shell particles (and combinations of internal and external mixing) in global climate models:

Kim, D., C. Wang, A. M. L. Ekman, M. C. Barth, and P. J. Rasch (2008), Distribution and direct radiative forcing of carbonaceous and sulfate aerosols in an in- teractive size-resolving aerosol–climate model, J. Geophys. Res., 113, D16309, doi:10.1029/2007JD009756.

Klingmüller, K., Steil, B., Brühl, C., Tost, H., and Lelieveld, J.: Sensitivity of aerosol radiative effects to different mixing assumptions in the AEROPT 1.0 submodel of the EMAC atmospheric-chemistry–climate model, Geosci. Model Dev., 7, 2503-2516, doi:10.5194/gmd-7-2503-2014, 2014.

The references have been added, thanks for the suggestions.

3. Technically, the generation of the synthetic BC aggregates is not outlined in detail. What code is used? Is it publicly available? If yes, this would improve the traceability of the results

The aggregate generation code has been developed by Dr. Richard Denis, as stated in the acknowledgment section. The code has been described and used by Scarnato ACP, 2013 and Richard et al. 2008 and 2011 (the latter for applications in Lunar science). The aggregates have been in detail characterized by several morphological descriptors. Any available aggregate generation model can be used to reproduce aggregates with the specifics described in the paper.

4. The aspect ratio of the synthetic dust particles is given, but what is the relation between all three side lengths/diameters of the rectangular prisms and ellipsoids? The terms "spheroid" and "ellipsoid" seem to be used synonymously here. However, if in fact spheroids are used (ellipsoids with two of three diameters being equal) as stated in l 6, p. 2496, this should be made clear in Table 1 and also, if they are oblate or prolate. Accordingly, please check the consistent usage and appropriateness of the term "rectangular prism".

The aspect ratio is kept constant at 1.75 for all 3 axes. The spheroids are oblates and the optical properties discussed are averages over 1000 random orientations. The text has been modified accordingly in Table 1.

5. In Fig. 1, BC and dust should be clearly distinguishable, e.g., by using different colour tints or markers.

We marked the BC particles with red circles on top the dust particles.

6. In Fig. 4, the results are indistinguishable. Colours could help.

As described in the text, the assembles of BC aggregates are characterized by MEC, MAC and MSC values of very similar magnitude and spectral dependency, resulting in little or no sensitivity to aggregate size, therefore lines are very close. Different colors and symbols have been not found to help, so the plots are left as submitted. Where differences on optical properties are more significant (i.e. Fig. 5), the black color used to identify BC aggregates does not create an issue in the readability of the plots.

7. In Fig. 8 (a) for BL2S3 the MAC seems to be plotted instead of the MEC. Generally, Fig. 8 is confusing because some curves and symbols are hard to identify; also the sub-captions only refer to the internally mixed case.

We checked and plots are consistent. The sub-caption has been modified with a) MEC b) MAC c) MSC

The only option to reduce the clutter in figure 8 would be to plot the three coefficient into two separate sets, one for larger and one for smaller particles, but that will make the comparison less direct, so we prefer to keep the plots as they are.

8. In Fig. 9, the results for S3 and S5 are drastically different from the results for S1 and S2. Because S2 and S3 differ only by a (moderate) change in the size of the dust particles, at first sight this looks surprising, however the discussion in the last paragraph of p. 2503 is vague. Is it possible to provide a simple qualitative explanation (e.g., does in l 26 "small particles sizes (small size parameter)" indicate that combining small BC particles and big dust particles to big internally mixed particles simply removes all particles from a size range of efficient extinction, analogously to the range 2 pi r / lambda ~ 4 for spherical particles)?

The difference in size between the cases S2 and S3 is not moderate considering the short spectral range (as a matter of fact the size parameter at 300 nm is almost 6 for case S2 and 16 for case S3). One should also consider the small ratio between the size of the internally mixed particle and the BC of 1.8 for BL2S1 and 2.8 for BL2S2, compared to 5 for BLS3 and 10 for BL2S5.

The authors modified the text after the sentence:

[…] We found that for smaller particles (cases S1, S2, BL2, BL2S1, BL2S2) external and internal mixtures predict similar values of Cabs, scat, ext in the entire spectral range, with ratios respectively of 1.09±0.06, 0.96±0.05 and 1.02±0.07.

in the following way:

"The latter might be due to the combination of 1. small electromagnetic interactions between the BC aggregate and the mineral dust particle, due to the small size parameter and, 2. the small difference in size between BC and mineral dust particles (with a mixture/core size ratio < 2.8). While, we found for larger particles (with larger size parameters) larger differences in $C_{ext, abs, scat}$ values, depending on the parametrization of the mixing configurations (such as external, cases BL2+S3, BL2+S5, BL2S3, and internal BL2S3 and BL2S5). For those cases, simulations using external mixture representations give smaller Cabs values compared to internal mixtures (with average ratio of 0.87±0.30) for wavelengths shorter than 550 nm, while larger values (average ratio of 1.35±0.49) for wavelengths larger than 550 nm. Further, Cscat values for external mixtures are smaller than internal mixtures in most of the spectral range studied (and similarly for Cext values) with average ratios of 0.59±0.30 and 0.49±0.27 for wavelength shorter and larger than 550 nm. Internal mixture might lead to larger values in Cscat (and similarly for Cext) values because of larger scattering interactions and electromagnetic coupling between mineral dust and BC, which might lead to an increase in scattering compared to the external mixtures, similar results were found in Scarnato et al., 2013"

9. Table 5 and Fig. 11 are not explicitly referenced in the text (p. 2500, l 27 should probably refer to Table 5, not 4).

Thanks for noticing; we changed the Table number accordingly

10. Some typos are in the text, e.g.:
p. 2489, l 24: "indeces" should read "indices"
p. 2492, l 14: "same" should read "some"

p. 2495, l 24: "randomly" should read "random"
p. 2496, l 21: "indeces" should read "indices"
p. 2498, l 7: "Califonia" should read "California"
p. 2500, l 20: "asymmeter" should read "asymmetry"

We thank the reviewer for pointing out the typos, they have all been corrected.

Manuscript prepared for Atmos. Chem. Phys.

with version 3.2 of the LaTeX class copernicus.cls.

Date: 10 May 2015

Perturbations of the optical properties of mineral dust particles by mixing with black carbon: A numerical simulation study.

B.V. Scarnato[1], S. China[2], K. Nielsen[1], and C. Mazzoleni[2]

[1]Naval Postgraduate School, 589 Dyer Road, Root Hall, Monterey, CA-93943-5114, USA

[2]Michigan Technological University, Department of Physics and Atmospheric Sciences Program, 1400 Townsend Drive, Houghton, MI-49931, USA

Correspondence to: bvscarna@nps.edu

Abstract. Field observations show that individual aerosol particles are a complex mixture of a wide variety of species, reflecting different sources and physico-chemical transformations. The impacts of individual aerosol morphology and mixing characteristics on the Earth system are not yet fully understood. Here we present a sensitivity study on climate relevant aerosols' optical properties to various approximations. Based on aerosol samples collected in various geographical locations, we have observationally constrained size, morphology and mixing, and accordingly simulated, using the discrete dipole approximation model (DDSCAT), optical properties of 3 aerosols types: 1. bare black carbon (BC) aggregates, 2. bare mineral dust, and 3. an internal mixture of a BC aggregate laying on top of a mineral dust particle, also referred as polluted dust.

DDSCAT predicts optical properties and their spectral dependence consistently with observations for all the studied cases. Predicted values of mass absorption, scattering and extinction coefficients (MAC, MSC, MEC) for bare BC show a weak dependence on the BC aggregate size, while the asymmetry parameter (g) shows the ~~opposites~~opposite behavior. The simulated optical properties of bare mineral dust present a large variability depending on the modeled dust shape, confirming the limited range of applicability of spheroids over different types and size of mineral dust aerosols, in agreement with previous modeling studies. The polluted dust cases show a strong decrease in MAC values with the increase in dust particle size (for the same BC size), while an increase of the single scattering albedo (SSA). Further, particles with radius between 180 - 300 nm are characterized by a decrease in SSA values compared to bare dust, in agreement with field observations.

This paper demonstrates that observationally constrained DDSCAT simulations allow to better understand the

variability of the measured aerosol optical properties in ambient air, and to define benchmarks biases due to different approximations in aerosol parametrization.

1 Introduction

Black carbon (BC), a distinct type of carbonaceous aerosol particle, is produced by incomplete combustion of fossil and biomass fuels. BC is a strong light absorber and therefore can contribute to atmospheric warming and surface dimming. Estimates of direct BC radiative forcing (DRF) are highly uncertain and range from 0.2 to 1.2 Wm^{-2} at the top of the atmosphere (TOA) (*Bond et al.*, 2013). Two main sources of DRF uncertainty are: 1. estimates of BC spatial distribution and 2. interaction of BC with electromagnetic waves (EMW) upon emission and after aging in the atmosphere. Realistic modeling of BC spatial distribution relies on proper parametrization of emission, life time and vertical distribution (*Samset et al.*, 2013; *Bond et al.*, 2013), while appropriate modeling of BC interaction with EMW relies on proper parameterization of aerosol shape, chemical composition and state of mixing with other aerosol compounds. Comparison between predicted spatial concentrations of BC from chemical transport models and AERONET measurements, shows consistent biases. In the specific, the fraction of aerosol column (extinction) attributable to absorption, the Aerosol Absorption Optical Depth (AAOD), is generally underestimated by models compared to values retrieved by AERONET (*Bond et al.*, 2013; *Koch et al.*, 2009; *Kim et al.*, 2008; *Klingmüller et al.*, 2014). The sources of discrepancy are not well understood~~;~~. In order to estimate BC DRF 'consistently' with observations, scaling factors of the order of 2-3, need to be introduced to BC emission estimates to match observed AAOD values. In *Koch et al.* (2009) BC predictions from the AeroCom model inter-comparison project showed a low model bias for AAOD, but an overestimation of surface and upper BC concentrations at lower latitudes. The authors suggest that most models are underestimating BC absorption and recommend to work on improving estimates of refractive indeces, particle size, and optical effects of BC mixing. Many transport models assume BC to be externally mixed with other aerosol compounds, while few models assume that BC is homogeneously internally mixed with other aerosol compounds (*Bond and Bergstrom*, 2006; *Koch et al.*, 2009). Differences in the representation of the aerosol mixing (i.e., BC with non absorbing aerosols) lead to different absorption values, which compared to measurements are too small in the case of external mixing and too high for the case of homogeneous internal mixing. Less often an encapsulation of a spherical and homogeneous absorbing core surrounded by a spherical and homogeneous non-absorbing host material is adopted (core-shell configuration), which gives more realistic magnitudes of absorption (*Jacobson*, 2014, 2001).

Despite that, not always core-shell configuration can represent the absorption variability in the laboratory and field observations (*Adachi et al.*, 2010; *Bueno et al.*, 2011; *Bond et al.*, 2013; *Cappa et al.*, 2012b,a). The latter might be due to the miss-representation of the BC particle aggregation and mixing, as shown by more detailed light scattering modeling studies performed by *Kahnert* (2010b); *Scarnato et al.* (2013) and *Adachi and Buseck* (2013). Recent studies show that internal mixing of BC with other aerosol materials in the atmosphere can alter its aggregate shape (*Zhang et al.*, 2008; *Xue et al.*, 2009; *Cross et al.*, 2010; *China et al.*, 2013), absorption of solar radiation (*Bueno et al.*, 2011; *Cappa et al.*, 2012b), and radiative forcing (*Adachi et al.*, 2010; *Kahnert et al.*,

2012). *China et al.* (2014), further, characterized the predominant mixing and morphology types observed with the electron microscopes from samples collected in different locations and for different sources (i.e., biomass burning aerosol and vehicle exhaust) by classifying BC into four main classes (bare BC, inclusions, thinly coated and embedded BC); similar classes where identified by *Scarnato et al.* (2013) for laboratory generated mixtures of BC and sodium chloride (an aerosol mixture resembling dirty marine aerosol).

Several field campaigns have been showing the occurrence of internal mixing of BC with dust aerosols in the accumulation mode (e.g., *Clarke et al.*, 2004; *Liu et al.*, 2008). During transport and aging in the atmosphere, various processes can result in the formation of multi-component aerosols containing dust, including: i) heterogeneous chemistry, ii) adsorption of water vapor on dust particle surfaces, iii) cloud processing, iv) coagulation of dust with other aerosol or cloud particles (see *Usher et al.* (2003)). On a global scale, bare dust is estimated to cool the Earth atmosphere. Mineral dust TOA DRF constitutes, as BC aerosols, one of the major uncertainties in climate studies (- 0.6 to 0.4 Wm^{-2}) due to the lack of knowledge of both dust spatial distribution and interaction with EMW. Parametrization of mineral dust optical properties is also a complex problem, as its optical properties are a strong function of i) the relative abundance of various minerals, ii) how the minerals are mixed together in an aerosol particle, and iii) the particle shape. Those factors depend on dust origins, and therefore on the elemental composition of surface soils, but also on dust lifting production mechanism, and dust chemical and physical transformations (i.e., compositional separation) during aging and transport in the atmosphere. Many field studies reported changes in composition during dust transport (i.e., *Prospero et al.*, 1981; *Chester and et al.*, 1972; *Hansell Jr. et al.*, 2011; *Nousiainen*, 2009). Observations from the ground and from aircraft over the Sahara show considerable variation and uncertainty in the optical properties of mineral dust (*McConnell et al.*, 2010; *Sokolik and Toon*, 1999). The large variability is attributed to the mineral dust particles variability in size distributions, chemical composition and morphology. Further, different modeling studies on light interaction with mineral dust aerosol show: i) the limited range of applicability, over different types of mineral dust aerosols, of commonly used shapes such as sphere (adopted in Mie computations) and spheroids (adopted in T-matrix computations and in AERONET retrieval) (*Merikallio et al.*, 2011), ii) the inability of Mie simulations to accurately reproduce the magnitude and wavelength peak positions of the mass absorption/extinction coefficients common for angularly shaped particles (as shown by *Hansell Jr. et al.* (2011) in the infrared region), and iii) the effect of non-spherical dust particles on the total RF is 55/5% (ocean/land) at the TOA and 15% at the bottom of the atmosphere (BOA) for both land and ocean, while local radiative heating within a dust plume causes enhancements of 20% of RF (*Otto et al.*, 2011).

Internal mixing of mineral dust and BC aggregates has strong impact on the optical properties of originally externally mixed aerosol, on their radiative forcing (*Mishra et al.*, 2012; *Sokolik et al.*, 2001) and on spatial and temporal distribution of precipitations, for example, during the monsoon in Asia (*Lau and Kim*, 2006) or the African jet streams (*Reale et al.*, 2011).

An accurate parametrization of aerosol optical properties due to variability in morphology and mixing with other aerosol compounds is crucial for a number of disciplines involving not only radiative forcing analysis (*Bond et al.*,

2013) and global and regional aerosol modeling (*Samset et al.*, 2013; *Kahnert*, 2010b), but also aerosol-cloud interactions, visibility and precipitation forecast (*Lau and Kim*, 2006) and, further, remote sensing of atmosphere and ocean color (*Russell and Heintzenburg*, 2000; *Durkee et al.*, 2000; *Yoshida et al.*, 2013).

For example, retrievals of aerosol (and ocean) properties require assumption of: 1. scattering phase function, 2. single scattering albedo (SSA), 3. estimates of ozone absorption and molecular scattering, and 4. for satellite applications, estimates of surface reflectance/albedo. Both orbital and ground based remote sensing techniques use a pre-selected library of aerosol types in the analysis of radiometric data~~a pre-selected library of aerosol types with spherical shape (or in same cases spheroidal shape i. e. for AERONET) and the retrieval algorithm selects~~. The computations of optical properties for the library often make use of spherical shape assumptions. The assumptions of mineral dust particles shape may vary in the retrieval algorithms. AERONET retrieval assumes mineral dust particles to be spheroidal (*Dubovik et al.*, 2006), while MISR retrieval (version 16+) use spheroidal, grains, plates and spherical shapes (*Kalashnikova et al.*, 2013). The retrieval algorithms select an aerosol type based on the best fit to radiance measurements (i.e. *Deuze et al.*, 2001; *Hasekamp et al.*, 2011).

The capability of the satellite and AERONET aerosol global network to provide spatio-temporal distributions of both dust and BC at different spatial scales, relies on how well the aerosol library used in the retrieval 'fits' the aerosol mixture in the atmosphere; therefore, it is dependent on the accuracy of the retrieval assumptions on dust and BC optical properties. Therefore, non-sphericity and chemical anisotropy of the particles are sources of potential inaccuracy and biases of data product. These inaccuracies may affect the retrieval of aerosol characteristics, such as refractive index, size, aerosol optical depth, aerosol absorption optical depth, etc.. (e.g. *Scarnato et al.*, 2013, and references therein).

In this paper we present an "observationally-constrained" sensitivity study of the optical properties of BC aggregates internally mixed with mineral dust aerosols in the UV - IR spectral range (computationally intensive). The spectral range used in this study is of interest for applications in climate modeling, remote sensing of aerosol and ocean properties, and visibility forecast. Computations are performed using the Discrete Dipole ~~approximation~~ Approximation (DDA - DDSCAT7.3) (*Draine and Flatau*, 1994), a technique for modeling particles with complex shape, chains and aggregates with anisotropic mixing. DDSCAT is based on the direct solution of the Maxwell equations without reference to the wave equation, which is usually used in the treatment of light scattering by simple shapes, such as sphere and spheroids. Synthetic particle design for the DDSCAT calculations is based upon single particle electron microscopy of bare BC, bare dust and BC-dust internally mixed particles BC on the surface of a dust particle ~~)~~collected in the atmosphere from different locations of the globe.

2 Method

2.1 Description of the synthetic particles

Black Carbon Aggregates. We generate synthetic BC aggregates by aggregation of monomers in random walk (*Richard and Davis*, 2008; *Richard et al.*, 2011). The synthetic BC aggregates are characterized by a volume

equivalent radius (a_{eff} also defined as the radius of a sphere containing all the volume of the particle) between 82 - 144 nm, a constant monomer diameter of 40 nm and an open-chain like structure. Such values have been observationally constrained after processing electron microscopes images of several aerosol samples collected in field campaigns carried out in different geographical locations, such as California's Sacramento Valley (CARES), Pico Island Azores (PICO), Mexico City, Mexico (MILAGRO), Detling, England (ClearfLo), where internal mixture of BC and mineral dust have been observed.

The reader should be aware that the morphological characterization of the ambient aerosol is determined by processing 2-D electron microscope images on aerosol particles laying on a substrate and assuming orientational anisotropy over a statistically representative sample. Therefore, as a *minor secondary aspect of the paper*, we investigated the appropriateness of the standard method adopted in literature to estimate a morphological descriptor, such as monomers number, of BC aggregates by performing image processing of two-dimensional (2-D) projections of *synthetic* BC fractal aggregates. Image processing of synthetic BC fractal aggregates allowed, as well, to assure that the synthetic particles have similar 2-D properties to those collected in the atmosphere.

In this paper, we describe the BC aggregate morphology and chain like structure in terms of 1) fractal dimension, porosity (*Shen et al.*, 2008; *Scarnato et al.*, 2013) and convexity (as descriptors of the chain topology), 2) aspect ratio, and 3) roundness.

BC particles can be represented as fractals, where each particle is described as an aggregate with monomers of the same size, approximately obeying the following scaling law

$$N_i = k_0 (R_g / r_m)^{D_f} \tag{1}$$

Where N is the number of monomers per aggregate with $i = (estimated, true)$, R_g is the radius of gyration, r_m is the monomer radius, k_0 is the fractal prefactor, here used a value of k_0=1.6 (*Liu et al.*, 2008), and D_f is the mass fractal dimension.

R_g is the root-mean-square distance from the center of each monomer to the aggregate center of mass. As often it is difficult to measure N_{true} from 2-D projections, for particles with $D_f < 2$, N_{true} is typically estimated as the ratio of the projected area of the aggregate (A_a) and the mean projected area of a monomer (A_p) in the aggregate (*Oh and Sorensen*, 1997; *Samson et al.*, 1987).

$$N_i = K_a (A_a / A_p)^{\alpha} \tag{2}$$

Where α is an empirical projected area exponent and it has a typical value of 1.09, while k_a has a value of 1.15. The sensitivity of N_i on the values of α and k_a has been discussed previously (*China et al.*, 2014).

The aspect ratio (AR) of the fractal aggregate, is defined as the ratio of the major axis (A) to the minor axis (B). Larger values of the aspect ratio indicate a more elongated particle.

$$AR = \frac{A}{B} \tag{3}$$

The roundness of a fractal aggregate, is defined as the ratio of the projected area (A_a) of the particle to the area of a circle with a diameter equal to the maximum length (L_{max}) of the particle.

$$Roundness = \frac{4A_a}{\pi L_{max}^2} \tag{4}$$

The chain like structure has been characterized in terms of convexity, porosity and fractal dimension (see equation 1.) The convexity C (also known as solidity), is defined as the ratio of the A_a of the particle and to the area of the smallest convex polygon in which the particle is inscribed (convex hull polygon - CHP). The polygon is calculated based on the boundary enclosing the foreground pixels of a binary image using straight-line segments to each outermost point.

$$C = \frac{A_a}{CHP} \tag{5}$$

The porosity (P) of the fractal aggregates is defined by *Shen et al.* (2008)

$$P = 1 - [(\beta_2 + \beta_3 - \beta_1)(\beta_3 + \beta_1 - \beta_2)(\beta_1 + \beta_2 - \beta_3)]^{1/2} \tag{6}$$

where β_i = I_i/(0.4 ρ_1 V_1 a_{eff}^2) is a dimensionless quantity, I_i with $i = (1,2,3)$ is the moment of inertia tensor, ρ_1 is the density and V_1 the volume of BC aggregates (see (*Shen et al.*, 2008)).

Morphological descriptors of synthetic BC aggregates are calculated from projected images of 50 randomly particle orientations.

Mineral dust aerosol. The morphology of suspended mineral dust might take various forms, as natural dust is an aggregate of internally mixed minerals. Different field studies show AR median values ranging between 1.4 and 1.9 (*Chou et al.*, 2006; *Clarke et al.*, 2004; *Reid et al.*, 2003; *Kandler et al.*, 2006; *Dubovik et al.*, 2006; *Mishra et al.*, 2012). In this study, we modeled dust aerosols as spheroids and rectangular prisms with an intermediate aspect ratio (compared to the refereed literature) of 1.75, which has also been found in CARES, PICO, MILAGRO and ClearfLo field campaigns (see Table 3). We summaries the characteristics of the synthetic/modeled aerosol particles in Table 1. Dust particles with a smaller radius are representative of particle size distribution of long lived distant-transported accumulation-mode airborne dust. The largest radius is representative of the particles size near the dust emission sources.

Aerosol Type	Legend	**Target shape in study**	$\mathbf{a}_{eff}$ [nm]
Dust	S1, E1	Rectangular prism, Ellipsoid	180
	S2, E2	Rectangular prism, Ellipsoid	280
	S3, E3	Rectangular prism, Ellipsoid	500
	S4, E4	Rectangular prism, Ellipsoid	700
	S5, E5	Rectangular prism, Ellipsoid	1000
Black Carbon	BL1	BC aggregate with 70 monomers	80
	BL2	BC aggregate with 100 monomers	100
	BL3	BC aggregate with 200 monomers	120
	BL4	BC aggregate with 300 monomers	140
Mineral dust and BC	BL2S1	Rectangular prism mixed w BC (BL2+S1)	190
	BL2S2	Rectangular prism mixed w BC (BL2+S2)	290
	BL2S3	Rectangular prism mixed w BC (BL2+S3)	503
	BL2S5	Rectangular prism mixed w BC (BL2+S5)	1010

Table 1: Characteristics of the modeled aerosol particles. Dust particles have an aspect ratio for all 3 axes (AR) of 1.75 in all cases (oblate). The optical properties of dust, BC and mixtures were averaged over 1000 random orientations.

2.2 Computation of Optical Properties

We have numerically simulated the optical properties for an ensemble of bare mineral dust, bare open chain-like BC aggregates and internal mixtures of BC and mineral dust, see Table 1 . Optical properties of the binary mixtures are modeled using a DDA model (DDSCAT.7.3), see for model details *Draine and Flatau* (1994, 2010). Numerical simulations have been carried out at the specific spectral channels of the AERONET Cimel radiometer (340, 380, 440, 500, 675, 870, 1020 nm) plus at the 550 nm wavelength for comparison with literature values. Optical properties have been averaged over 1000 random orientations, reference refractive indeces are listed in Table 2.

Aerosol Compounds	Reference Refractive Indeces	Density [g cm^{-3}]
Black Carbon	*Chang and Charalampopoulos* (1990)	1.8
Mineral Dust	*Wagner et al.* (2012)	2.6

Table 2: References of the wavelength dependent refractive indices and density values used for BC and mineral dust. *Chang and Charalampopoulos* (1990) values at about 550 nm are 1.77 - 0.63i, which are lower than the value of 1.95 - 0.79i suggested by *Bond and Bergstrom* (2006).

The optical properties discussed in this study are:

1. The mass absorption, scattering and extinction coefficient (MAC, MSC and MEC)

$$MAC = C_{abs}/mass \tag{7}$$

$$MSC = C_{scat}/mass \tag{8}$$

$$MEC = C_{ext}/mass \tag{9}$$

$$mass = \rho\frac{4}{3}\pi a_{eff}^3 = \frac{4}{3}\pi(\rho_1 a_{1,eff}^3 + \rho_2 a_{2,eff}^3) \tag{10}$$

$$\tag{11}$$

where C_{abs}, C_{scat} and C_{ext} indicate the absorption, scattering and extinction cross sections, $\rho_{1,2}$ is the density (index 1 indicates BC and index 2 mineral dust). MAC and MSC are necessary to calculate the effects of mass concentrations simulated by chemical transport models on radiative transfer. MAC and single scattering albedo (SSA) (defined in equation 13) are relevant to determinate the balance between negative and positive forcing.

2. The aerosol absorption, extinction and scattering Ångström exponent (AAE, EAE, SAE) computed from the slope of the linear fit passing though MAC, MSC and MEC curves (in log-log scale). The AAE and EAE are typically used as indicators of aerosol type and size.

$$AAE = \frac{-\triangle log(MAC)}{\triangle log(\lambda)}; EAE = \frac{-\triangle log(MEC)}{\triangle log(\lambda)}; SAE = \frac{-\triangle log(MSC)}{\triangle log(\lambda)} \tag{12}$$

3. The single scattering albedo (SSA) calculated as:

$$SSA = C_{scat}(\lambda)/C_{ext}(\lambda); \tag{13}$$

where $C_{abs,scat,ext}(\lambda)$ are defined in equation 7.

4. The asymmetry parameter defined as:

$$g = 1/2\int_0^\pi \cos(\theta)\sin(\theta)\mathrm{P}(\theta)\mathrm{d}\theta \tag{14}$$

where P(θ) is the scattering phase function and θ is the scattering angle.

SSA and g are the two fundamental parameters necessary to perform calculations of aerosol radiative properties (e.g., *Chylek and Wong*, 1995).

3 Results

3.1 BC internally mixed with dust

We have observed BC internal mixing with suspended mineral dust (BC particles laying on top of dust particles) in various field campaigns. In Fig. 1, we show a composite of SEM images from aerosol samples collected: a) in an urban location 10 km north of downtown Mexico City (MILAGRO, March 2006), b) 40 km downwind of the Sacramento urban area in the forested Sierra Nevada foothills, Califonia, USA (*Zaveri et al.*, 2012), c) in a rural site in Detling, UK (ClearfLo, January-February, 2012), d) at Pico Mountain Observatory, Azores Islands (Portugal) in the North Atlantic Ocean (*Honrath et al.*, 2004; *Dzepina et al.*, 2014).

The morphological characteristics of the BC and mineral dust particles are summarized in Table 3. The values reported for BC are in agreement with *Adachi et al.* (2007).

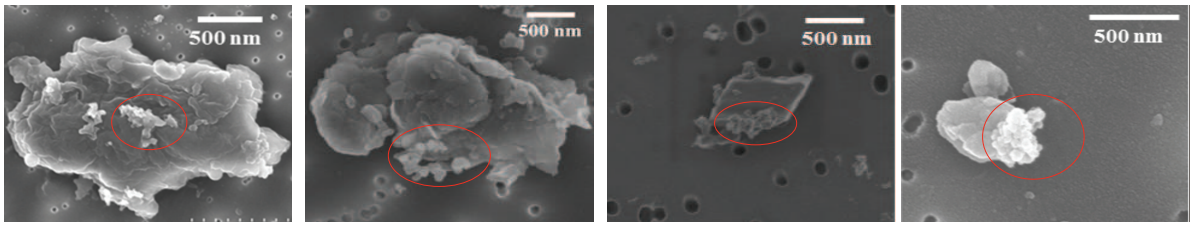

(a) *Milagro* (b) *CARES* (c) *ClearfLo* (d) *Pico*

Fig. 1: SEM images of internally mixed mineral dust and BC particles observed during various field campaigns, a) Mexico City, Mexico (Megacity Initiative: Local and Global Research Observations (MILAGRO) 2006); b) A silicon rich dust particle internally mixed with BC, Sacramento, Califonia, USA (2012); c) A complex internal mixture of multiple aerosol components Detling, UK (Clear Air for London (ClearfLo), 2012); and d) a dust particle with plate-like structure (clay-mineral) from Pico Mountain Observatory, Pico island, Azores (Portugal) in the North Atlantic Ocean (2012). Red circles identify BC on the surface of mineral dust particles.

Aerosol Type	Projected Area Equivalent Radius [nm]	AR	r_m [nm]
Dust	250 - 810	1.08 - 1.75	
Black Carbon	90 - 140	1.39 - 1.98	34 - 49

Table 3: Synthesis of morphological descriptors for BC and mineral dust aerosol particles sampled in various field campaigns.

3.2 Morphological characterization of the synthetic aggregates

In order to ensure that the shape of the synthetic BC aggregates are representative of ambient air samples, we processed the 2-D binary images of the synthetic particles at 50 random orientations. For synthetic aggregates presented in Fig. 2, we have estimated an average $N_{estimated}$ values ($\pm$ std deviation) of 63 ($\pm$8) for BL1, 119

(±13) for BL2, 179 (±12) for BL3 and 326 (±46) for BL4. Morphological descriptors for the cases BL1 to BL4 are summarized in Table 4. Aggregates have the same monomer size, similar chain structure, but increasing number of monomers.

The accuracy of $N_{estimated}$ values after image processing are conditional to two main factors: 1) the number of orientations taken for images processing, and 2) the size of the aggregate. In Fig. 3, we present a comparison of the $N_{estimated}$ values from the 2-D projected images with the actual N_{true} values used for the generation of the synthetic aggregates. The $N_{estimated}$ well approximate N_{true} within the uncertainties.

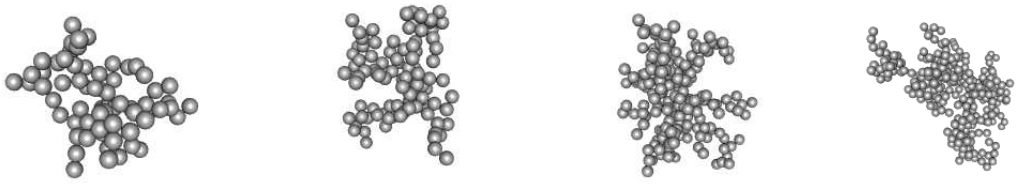

(a) *BL1* (b) *BL2* (c) *BL3* (d) *BL4*

Fig. 2: Representation of four BC aggregates (not in scale) with increasing number of monomers (see Table 4). In all cases the monomers radius is 20 nm.

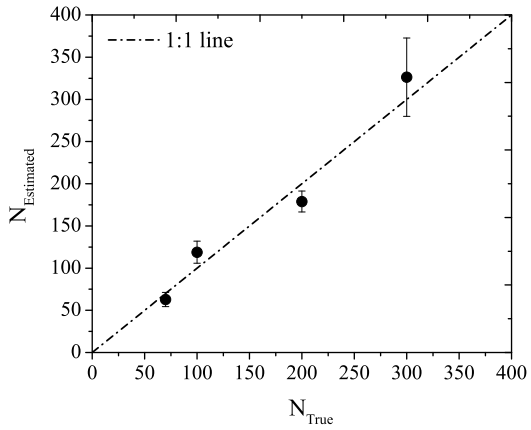

Fig. 3: Comparison between the actual monomers (N_{true}) number of the synthetic BC aggregates versus the estimated monomers number ($N_{estimated}$) after image processing of 2-D projections of 50 random aggregate orientations, the error bars represent the standard deviation.

3.3 Optical properties of bare BC aggregates

The spectral dependence of mass extinction, absorption and scattering coefficients (MEC, MAC, MSC) is presented in Fig. 4 for an ensemble of synthetic open chain-like aggregates, as described in Table 4 (and with a size

Case	$2r_m$ [nm]	N_{true}	a_{eff} [nm]	P	Convexity	D_f	AR	Roundness
BL1	40	70	82	0.86	0.65 ± 0.05	1.98 ± 0.09	1.36 ± 0.17	0.43 ± 0.08
BL2	40	100	100	0.92	0.66 ± 0.05	1.95 ± 0.05	1.46 ± 0.22	0.38 ± 0.04
BL3	40	200	126	0.89	0.63 ± 0.04	2.03 ± 0.05	1.34 ± 0.16	0.44 ± 0.05
BL4	40	300	144	0.90	0.60 ± 0.06	1.95 ± 0.07	1.74 ± 0.36	0.34 ± 0.07

Table 4: Morphological characterization of synthetic BC particle.

parameter X = 2 π a_{eff}/ $\lambda < 4.5$). Large difference are found in optical properties of BC aggregates compared to equivalent volume spherical particles, biases in the numerical simulations and relevance for radiative forcing estimates are discussed in *Scarnato et al.* (2013); *China et al.* (2015).

It is well known that bare/uncoated fresh BC absorbs more radiation, than scatters (*Bond et al.*, 2013). Therefore, MAC represents the dominant contributor to the MEC. *Bond et al.* (2013) report BC MAC values larger than 5 m^2/g. Predicted values of MEC, MAC and MSC (see equation 7) are shown in Fig. 4 for a composite of BC aggregates with similar porosity and monomers size, but increasing monomers numbers, see Table 4. MAC values are strongly wavelength dependent (see also *Moosmueller et al.* (1998) and *Lack and Langridge* (2013)). At 550 nm MAC predicted values, using a BC density (ρ) of 1.8 g/cm^3 (*Bond and Bergstrom*, 2006), range between 5.32 and 5.65 $m^2 g^{-1}$ and they are not strongly sensitive to the aggregate size. The latter finding is in agreement with the fractal theory by *Berry and Percival* (1986), which maintains that mass absorption coefficient should not be a strong function of the size, but rather a strong function of the refractive index, physical shape (and mixing) (e.g. *Fuller et al.*, 1999; *Liu et al.*, 2008; *Scarnato et al.*, 2013).

The range of predicted MAC values at 550 nm is in agreement with field measurements by *Clarke et al.* (2004) and modeled values by *Kahnert* (2010a) and *Kahnert and Devasthale* (2011).

However, several studies (e.g., *Bond and Bergstrom*, 2006; *Adachi et al.*, 2007; *Cross et al.*, 2010) reports larger values. Reasons might be related to different index of refraction or density values, for instance, the values predicted here are lower than the published values at 550 nm by *Scarnato et al.* (2013) because of differences in the adopted refractive indices. At a wavelength of 550 nm, the refractive index by *Chang and Charalampopoulos* (1990), adopted in these simulations, have lower real and imaginary indices than the value of 1.95 - 0.79i recommended by *Bond and Bergstrom* (2006) (see Table 2), which was adopted in simulations by *Scarnato et al.* (2013). In this study, as in *Scarnato et al.* (2013), we used a BC ρ_1 value of 1.8 g cm^3. If we use a value of ρ_1 equal to 1.4 g/cm^3 and *Chang and Charalampopoulos* (1990) refractive index, we find for the cases BL1 to BL4 MAC values at 550 nm of about 7 m^2/g. As a reminder, the OPAC code uses a density value as low as 1 g/cm^3 for BC. MSC and SSA values, as shown in Fig. 5, are slightly more sensitive to the aggregates size than to the MAC (see also *Scarnato et al.* (2013) for the SSA dependence on aggregate compactness). SSA values are lower than those predicted by *Scarnato et al.* (2013), due as well to the differences in the refractive indices used in the simulations. The SSA magnitude and spectral variation presented in this study are both in agreement with laboratory measurements by

Sharma et al. (2013). At 550 nm, SSA shows little variability through case BL1 to BL4 with an average value of 0.19 ± 0.02. Just looking at MAC and MEC, one could argue that the implementation of optical properties of bare BC aggregates in chemical transport and radiative transfer models might be greatly facilitated by the fact that some of the properties of BC aggregates are little sensitive to aggregate size in the UV, VIV and NIR. Such a property would reduce the need for complex parametrizations of BC aggregates optical properties to accurate modeling of the chain structure, and monomer size of the aggregate (see (*Liu et al.*, 2008) for sensitivity to monomer size). This assumption fails when looking at the asymmeter parameter (g) spectral dependency for the cases BL1 to BL4 in Figure 5 b), where g presents a strong sensitivity to the BC aggregate size in the entire spectral range under study. In Fig. 5, DDSCAT predicts the lowest g values for the BL1 case, intermediate values for the case BL4 and higher values for cases BL2 and BL3. For wavelenghts longer than 800 nm the differences in g values between the cases BL2, BL3 and BL4 are minimised.

AAE, EAE and SAE values are wavelength dependent, see Table ~~4 and~~5 and*Scarnato et al.* (2013). In the spectral range between 340-1600 nm, AAE values are consistent with observations and theoretical results with values of approximately 1, while in the spectral range between 400-675 nm AAE values approach 1.2 (in agreement with *Lack and Langridge* (2013)). The range of values of AAE, EAE and SAE is also fairly consistent with *Sharma et al.* (2013). For example, we found a SAE average value of 1.79 ± 0.37, which is in the range of values reported by *Sharma et al.* (2013) of 1.61 ± 0.05, and by *Gyawali et al.* (2012) of 1.88.

Case	AAE a (b) (c)	EAE a (b) (c)	SAE a (b) (c)	MAC(550) m^2/g^{-1}	MEC(550) m^2/g^{-1}	SSA(550)	g(550)
BL1	1.26 (1.24) (1.04)	1.36 (1.33) (1.15)	1.49 (1.32) (1.82)	5.60	6.80	0.17	0.42
BL2	1.24 (1.23) (1.11)	1.38 (1.41) (1.26)	1.58 (2.20) (2.32)	5.72	6.93	0.17	0.60
BL3	1.18 (1.21) (1.05)	1.29 (1.32) (1.18)	1.33 (1.73) (1.90)	5.38	6.94	0.22	0.73
BL4	1.18 (1.18) (1.04)	1.27 (1.35) (1.15)	1.60 (1.92) (1.70)	5.53	6.98	0.20	0.76

Table 5: Summary of optical properties predicted by DDSCAT for bare BC aggregates at 550 nm. AAE and EAE have been calculated in different wavelength ranges: a) 340-1000 nm, b) 400-675nm (and c) 340 - 1600 nm - (spectral range not shown in Fig. 4). MAC and MEC values are provided at 550 nm. MSC values have not been included in the table, as they can be calculated by the difference between MEC and MAC values.

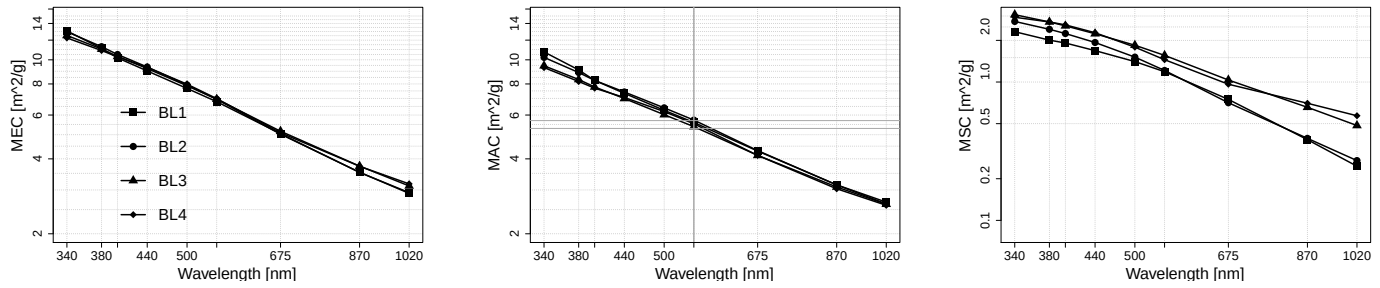

(a) *MEC of bare BC* (b) *MAC of bare BC* (c) *MSC of bare BC*

Fig. 4: (a) MEC (b) MAC (c) MSC spectral dependency (in log-log scale) for an ensemble of BC aggregates, as described in Table 1. All the computed optical values are averaged over 1000 particle orientations. Dark grey lines underlines MAC values at 550 nm. Note that the y scale is different in the 3 plots.

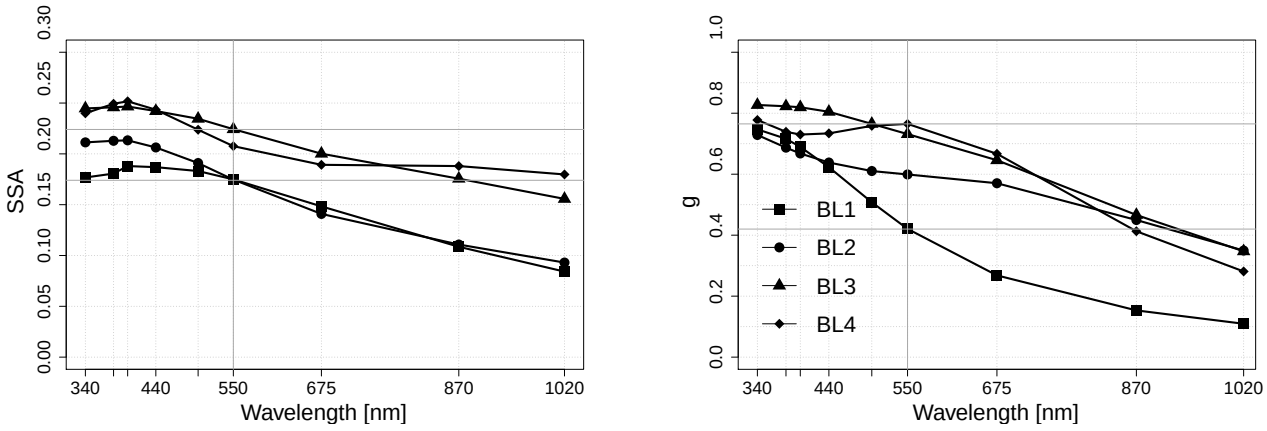

(a) *SSA of bare BC* (b) *g of bare BC*

Fig. 5: a) SSA and b) g spectral dependency for bare BC aggregates (Cases BL1, BL2, BL3, BL4). All the computed optical values are averaged over 1000 particle orientations.

3.4 Optical properties of mineral dust

In all the field campaigns presented here, we have found mineral dust particles with jagged surfaces and irregular shape (see Fig. 1). In particular, in Fig. 1 a), c), d) dust particles were found to be silica rich and with a plate-like morphology. We found that the DDSCAT predicted optical properties have a large variability depending on the modeled dust shape, despite having the same aspect ratio. In Fig. 6, we present the residual of the $Q_{abs,scat,ext} = C_{abs,scat,ext}/\pi a_{aeff}^2$ for an ensemble of spheroids ($E1, E2, E3, E4, E5$) and rectangular prisms ($S1, S2, S3, S4, S5$) with AR = 1.75. The difference in the $Q_{abs,scat,ext}$ is small for case $E1$ and $S1$, and it is larger (up to about 50% in the $Q_{ext,scat}$ at 550 nm) for larger particle sizes (cases S4, S5).

The sensitivity of $Q_{abs,scat,ext}$ to shape confirms the limited range of applicability of spheroids over different types and size of mineral dust aerosols, in agreement with previous modeling studies *Merikallio et al.* (2011); *Hansell Jr. et al.* (2011); *Otto et al.* (2011). Extended studies on the sensitivity to shape of mineral dust particles optical properties in the UV-NIR can provide useful constrains on the envelope of values to be expected during measurements in ambient air (i.e., *Sokolik and Toon*, 1999; *Hansell Jr. et al.*, 2011). From Fig. 6, it is also evident that simplifications, in handling mineral dust particle shape, can generate positive (and at times negative) biases in retrieved AOD and opacity, when ellipsoids are adopted in the retrieval and aerosol at the site resemble more the synthetic rectangular prisms/modeled particles. The magnitude of the biases are strictly dependent on the wavelength and size of the particles. For example, if aerosols at the site resemble more the rectangular prism than ellipsoidal shape, large positive biases (up to 50%) in retrieved AOD can be expected at 550 nm for particles with an a_{eff} between 700 and 1000 nm, as mineral dust particles (cases S4, S5) modeled as rectangular prisms have a higher Q_{ext} than ellipsoids (cases E4, E5). No AOD biases should be expected at 550 nm depending on the two shape assumptions for particles smaller than 700 nm. While, an average AOD bias of 15 $\pm$7 % in the shorter wavelength range (340-500 nm) and 10 $\pm$13 % for longer wavelengths range (550 - 1020 nm) should be expected.

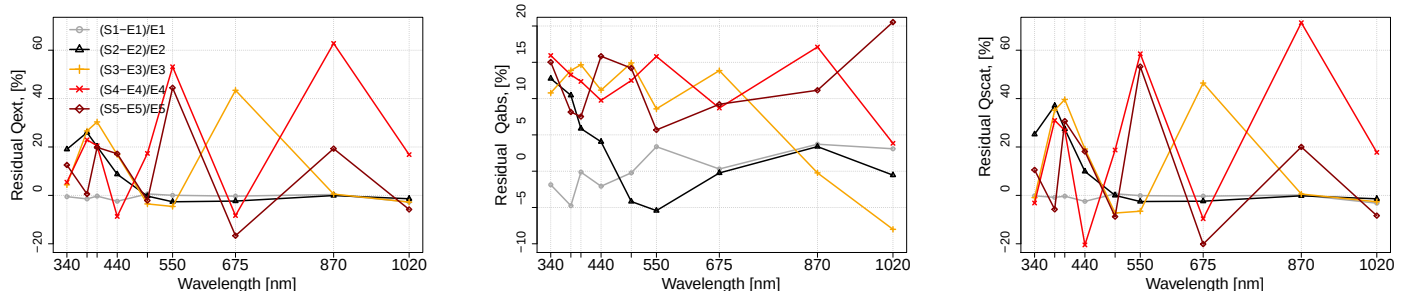

(a) *Qext of Mineral dust* (b) *Qabs of Mineral dust* (c) *Qscat of Mineral dust*

Fig. 6: Differences in percentage between extinction, absorption and scattering efficiency for spheroids vs. rectangular prisms.

3.5 Optical properties of BC aggregates internally mixed

We have modeled a binary internal mixtures of BC aggregates and mineral dust, as visualized in Fig. 7. The BC aggregates is on the surface of the mineral dust particle. Given the plate like structure of Fig. 1 a), c) and d), we opted to model mineral dust shape as rectangular prisms. The chosen shape does not cover the whole range of variability encountered in ambient air, but for our cases (see Fig. 1, it adds a degree of complexity in the description of mineral dust shape compared to ellipsoids).

Fig. 7: Visual representation of polluted dust, as an internal mixture of BC and mineral dust. The shape of the particle is repressented by an array of coordinates (small dots or spheres), to which is associated a dipole moment. Brown dots represent the dust particle dipoles, while grey small spheres represent the dipoles of the BC aggregate. The cases BL2S1, BL2S2, BL2S3, BL2S5 have BL2, respectively, on the surface of S1, S2, S3 and S5. Arrows show that sides of the rectangular prism can vary keeping aspect ratio constant to a value of 1.75.

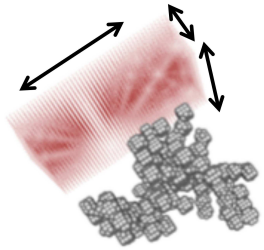

In Fig. 8, we present the MAC, MSC, MEC spectral dependency for 3 different aerosol types: 1) an ensemble of bare mineral dust particles with aspect ratio of 1.75 and increasing size (cases S1 trough S5), 2) one bare BC aggregate (case BL2), and 3) internal mixtures of the two types (cases BL2S1 trough BL2S5, where BL2 is mixed respectively with S1, S2, S3, and S5).

Bare mineral dust aerosol (see cases S1 through S5 in Fig. 8) have low MAC values compared to bare BC aggregates (i.e., case BL2 in Fig. 8) in the UV and NIR region. The MAC values of bare dust are wavelength dependent with predicted larger values in the UV-VIS. Smaller dust particles have higher MAC. DDSCAT predicts for bare/unpolluted dust at 550 nm an MAC average value of 0.13 ± 0.03 m^2g^{-1} ($\pm$ standard deviation).

The internally mixed particles (cases BL2S1 through BL2S5, also refereed as polluted dust) have higher MAC values for smaller particles (BL2 has the highest MAC). As expected, DDSCAT predicts higher MAC values for polluted dust than unpolluted/bare dust, with an average MAC value of 0.26 ± 0.27 m^2g^{-1} at 550 nm.

Further, MSC values of bare mineral dust aerosols have a strong variability with size and wavelength. DDSCAT predicts an average MSC value at 550 nm of 2.1 ± 1.9 m^2g^{-1} for dust particles ranging in size from 0.18 to 1 micron. When considering just the accumulation mode, with dust size ranging between 0.5 and 1 microns, DDSCAT predicts a smaller MSC average value of 0.8 ± 0.2 m^2g^{-1}. Fine mode particles compared to coarse mode particles have larger MSC values because smaller particles scatter light more efficiently at visible wavelengths. *Hand and*

Malm (2007), after reviewing 60 studies of ground based observations, report at 550 nm for the fine mode dust an average MSC value of 3.3 $\pm$ 0.6 m^2g^{-1}, while they report in the accumulation mode smaller MSC values of 0.9 $\pm$ 0.8 m^2g^{-1}, in agreement with our study. The MSC of larger dust particles (cases S3, S4, S5) does not show a strong spectral dependency, while the opposite is true for small particles (cases S1 and S2), see Fig. 8 c). It should be noted that the spectral variability of AOD is used in remote sensing in interpreting aerosol type. For example, mineral dust aerosol is assumed to have a "spectrally flat" AOD, while biomass burning or polluted aerosol usually exhibit a strong wavelength dependence. The spectral dependencies in Fig 8 a) demonstrates that small mineral dust aerosol particles and polluted dust have also a strong AOD spectral dependence, those characteristic might be a potential source of classifications of aerosol type, size and amount.

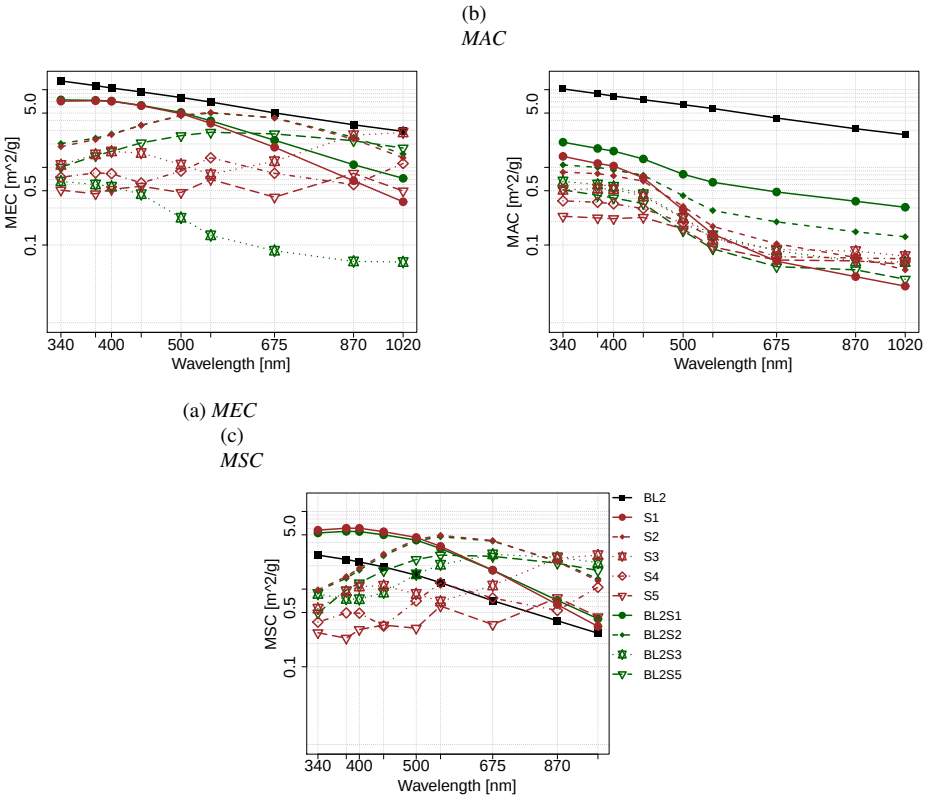

Fig. 8: (a) MEC (b) MAC (c) MSC spectral dependency for a BC aggregate (BL2) internally mixed with a mineral dust particle represented as a rectangular prism (BL2S1-BL2S5), see Fig. 7. MEC, MAC, MSC are normalized *by total mass* of the internally mixed particle, see Table 2). All the computed optical values are averaged over 1000 particle orientations.

Further, representation of the state of aerosol mixing, whether internal (such cases BL2Si with i=(1,2,3,5)) or external (such as cases BL2 plus Si i=(1,2,3,5)) might affect the overall optical properties of the aerosols, see Fig. 9. We found that for smaller particles (cases S1, S2, BL2, BL2S1, BL2S2) external and internal mixtures predict similar values of $C_{abs,scat,ext}$ in the entire spectral range, with ratios respectively of 1.09$\pm$0.06, 0.96$\pm$0.05 and 1.02$\pm$0.07.

The latter might be due to the combination of 1. small electromagnetic interactions between the BC aggregate and the mineral dust particle ~~and small particles sizes (small size parameter,~~ due to the small size parameter and, 2. the small difference in size between BC and mineral dust particles (with a mixture/core size ratio smaller than 2.8). While, we found ~~larger differences in predicted~~ for larger particles (with larger size parameters) larger differences in $C_{ext,abs,scat}$ values, ~~when BL2 is mixed externally or internally with larger mineral dust particles (~~depending on the parametrization of the mixing configurations (such as external, cases BL2+S3, BL2+S5, BL2S3, and internal BL2S3 and BL2S5). For those cases, simulations using external ~~mixtures~~ mixture representations give smaller C_{abs} values compared to internal mixtures (with average ratio of 0.87~~±0.30~~±0.30) for wavelengths shorter than 550 nm, while larger values (average ratio of 1.35~~±0.49~~±0.49) for wavelengths larger than 550 nm. Further, C_{scat} values ~~of~~ for external mixtures are smaller than internal mixtures in most of the spectral range studied (and similarly for C_{ext} values) with average ratios of 0.59~~±0.30~~ ±0.30 and 0.49~~±0.27~~ ±0.27 for wavelength shorter and larger than 550 nm. Internal mixture might lead to larger values in C_{scat} (and similarly for C_{ext}) values because of larger scattering interactions and electromagnetic coupling between mineral dust and BC, which might lead to an increase in scattering compared to the external mixtures, similar results were found in (*Scarnato et al.*, 2013).

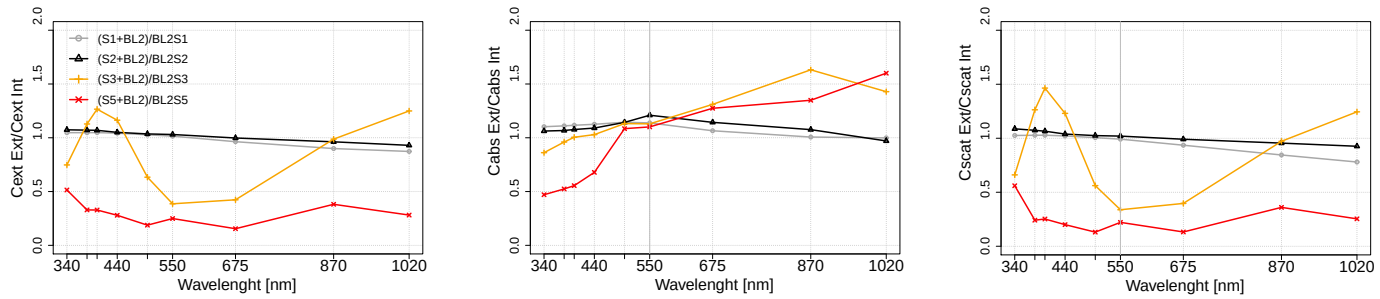

(a) C_{ext} *ratio* (b) C_{abs} *ratio* (c) C_{scat} *ratio*

Fig. 9: (a) C_{ext}, (b) C_{abs} and (c) C_{scat} ratios of an external vs. internal mixture of BC and mineral dust aerosols.

The SSA spectral signatures of bare BC (BL2), an ensemble of mineral dust (cases S1 through S5), and internal mixtures of the two aerosol components (BL2S1 through BL2S5) are shown in Fig 10. Bare mineral dust (case S1 trough S5) show a typical decrease in the SSA magnitude for wavelengths shorter than 500 nm, with SSA values ranging from 0.85 to 0.96 depending on the size of the dust particle, with smaller values attributed to larger particles. The range of values predicted by DDSCAT, in this study, is in agreement with values of 0.7 to 0.97 for Sahara dust reported by *Ryder et al.* (2013), where the authors attributed variability in measured values to the presence of a significant number of large particles. Further, analyses of the SSA values of Saharan dust from the Aerosol Robotic Network (AERONET) reported averages of 0.95 at 0.67 microns (*Dubovik et al.*, 2002). SSA values of $0.95 - 0.99$ have been reported during the Saharan Dust Experiment (SHADE) and the Dust Outflow and Deposition to the Ocean (DODO) (*Tanre et al.*, 2003; *McConnell et al.*, 2010; *Johnson et al.*, 2008). *Osborne*

et al. (2008) estimated the SSA for pure dust aerosol during the Dust and Biomass-burning Experiment DABEX, (*Haywood et al.*, 2008) to be consistently high (ranging between $0.98 - 0.99$).

For wavelengths shorter than 500 nm, small polluted dust particles (BL2S1 - BL2S2) show a stronger decrease in the SSA magnitude compared to unpollutted dust particles (S1 - S2), perturbation of dust optical properties of the same order of magnitude was also found in the Aerosol Characterization Experiment (ACE) field campaign (*Clarke et al.*, 2004). While DDSCAT predicts for internally mixed particles larger than 500 nm (BL2S3-BL2S5) an increase of SSA at all wavelengths compared to bare dust particles (S3-S4-S5). Such a "cut off" in SSA values is due to the fact that simulations predict for small internally mixed particles (cases BL2S1 and BL2S2), where dust particles are small in size, a steep increase in the absorption and no significant variation in the scattering properties compared to bare mineral dust (S1-S2). The latter leads to smaller SSA values of internal mixtures compared to bare mineral dust particles. Further, when mineral dust particles are large (cases S3-S5), and therefore the BC mass (case BL2) results comparatively much smaller than the mass of case S3 and S5), DDSCAT simulations predict a steep increase in the scattering, but less in the absorption, therefore prevailing scattering vs. absorption, for those cases are associated with larger SSA values compared to bare mineral dust.

In an attempt to synthesize the differences between the above discussed optical properties of bare BC and internal mixtures, we found that:

With the increase in size of mineral dust the absorption increases; however, also the scattering of the internal mixture (cases BL2S1 BL2S5), increases leading to larger SSA values for internal mixtures compared to bare BC (case BL2) (not shown here, as we provide MAC normalized by the total mass of the particle, not just BC mass). The increase in the absorption, despite no embedding (no "lens effect") , see also(*Scarnato et al.*, 2013), is due to absorption properties of mineral dust.

DDSCAT predicts a wavelength dependent asymmetry parameter g, BC has higher spectral dependency than dust, mostly due to the variation in real part of the BC refractive index with wavelength. DDSCAT predicts at 550 nm higher g values for internally mixed polluted dust than bare mineral dust; larger g values are predicted when modeling an external mixture compared to external mixture, differences can amount up to about 37% (see Table 6).

Case	a_{eff} [nm]	AAE a (b)	EAE a (b)	SEA a (b)	MAC(550) m^2/g^{-1}	MEC(550) m^2/g^{-1}	SSA(550nm)	g(550nm)
S1	180	3.92 (5.68)	2.8 (2.62)	2.75 (2.37)	0.14	3.70	0.96	0.75
S2	284	2.90 (4.16)	0.22 (0.95)	0.25 (1.56)	0.17	5.10	0.96	0.81
S3	500	2.15 (3.70)	0.65 (0.80)	1.17 (0.18)	0.12	0.82	0.85	0.60
S4	700	1.89 (3.13)	0.10 (0.47)	0.69 (1.5)	0.13	1.32	0.90	0.79
S5	1000	1.53 (2.60)	0.18 (0.26)	0.74 (0.60)	0.10	0.70	0.86	0.81
BL2S1	190	1.84 (2.39)	2.20 (2.23)	2.46 (2.19)	0.64	3.97	0.84	0.77
BL2S2	289	2.00 (2.48)	1.08 (0.14)	0.27 (1.63)	0.27	5.00	0.94	0.81
BL2S3	503	2.10 (3.17)	0.19 (0.93)	0.34 (2.68)	0.13	2.19	0.94	0.79
BL2S5	1010	2.68 (4.20)	0.45 (0.97)	0.92 (1.48)	0.09	2.82	0.96	0.88

Table 6: Summary of simulated optical properties for Mineral Dust and internal mixtures with BC aggregates. AAE and EAE have been calculated in two different wavelength range: a) 340-1020 nm and b) 400-675 nm.

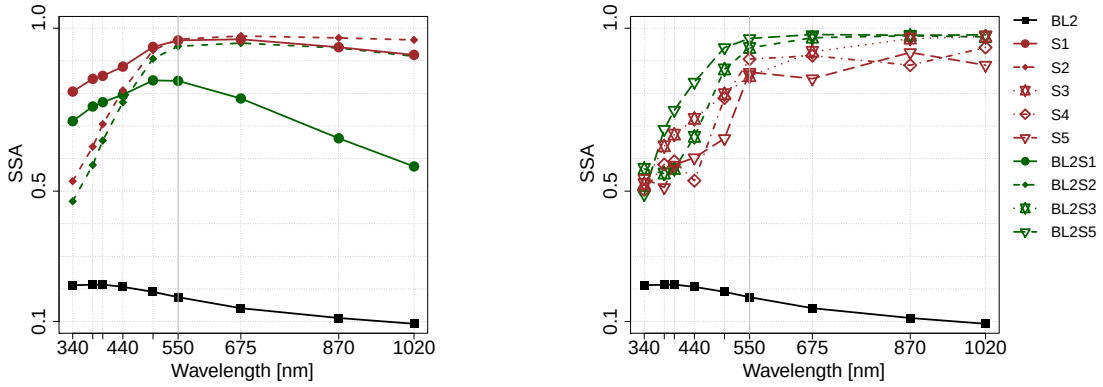

(a) *SSA spectral dependency for smaller particles size*

(b) *SSA spectral dependency for larger particle size*

Fig. 10: SSA for different particle sizes in the accumulation mode: (a) finer particles (b) larger particles .

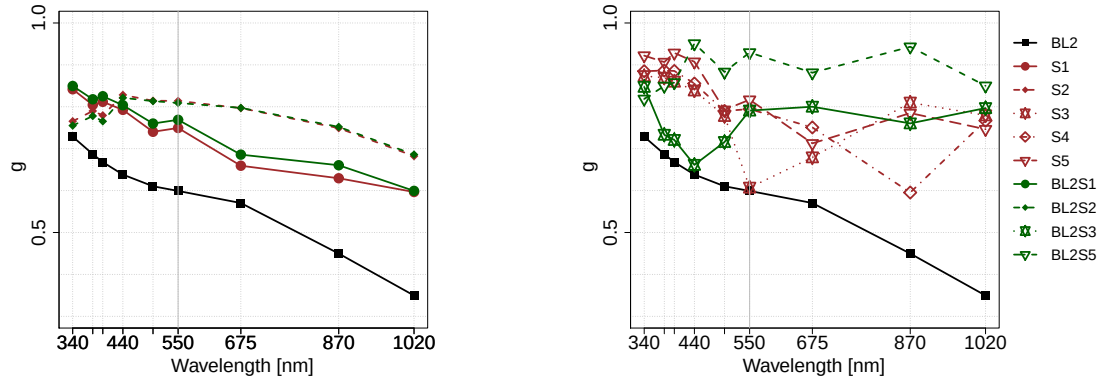

(a) *g spectral dependency for smaller dust particles size*

(b) *g spectral dependency for larger dust particle size*

Fig. 11: g for different particle sizes in the accumulation mode: (a) finer particles (b) larger particles .

4 Conclusions

Microscopes images of ambient air aerosol samples collected in various locations of the globe show occurrence of internal mixture of BC aggregates and mineral dust aerosols, see also (*Clarke et al.*, 2004; *Haywood et al.*, 2008). The aerosols shape/morphology and state of mixing, whether internal or external can affect the interaction with EMW and the overall optical properties of the aerosols mixtures, contributing therefore to uncertainty in 1. DRF estimates, 2. validation of chemical transport models with remote sensing measurements, 3. visibility forecast and 4, spatial and temporal distribution of precipitations and their forecast.

In this study, we carried out numerical simulations to investigate on the sensitivity of climate relevant aerosols optical properties to various approximations on aerosol size, shape and state of mixing, and draw benchmarks considerations for climate studies and remote sensing applications. Based on aerosol samples collected in Mexico, England, USA (California) and Portugal, we have observationally constrained morphology and mixing, and modeled optical properties accordingly, of 3 different types of aerosols: 1. bare BC aggregates, 2. bare mineral dust, and 3. an internal mixture of BC and dust particles, also referred as polluted dust.

Optical properties including $MAC, MEC, MSC, AAE, EAE, SSA$ and g were predicted over the spectral range between 340 and 1020 nm using DDSCAT, which applies the discrete dipole approximation (DDA). Specific wavelengths have been selected to match the AERONET nominal channels.

Key results for bare BC aggregates include: i) a weak MAC dependency on the aggregate size, but stronger MAC dependency on the refractive index, in agreement with *Berry and Percival* (1986); *Liu et al.* (2008); *Scarnato et al.* (2013); ii) a strong g dependency on aggregate size; iii) consistency between DDSCAT predicted and observed values of both AAE, EAE, SAE (e.g., *Lack and Langridge*, 2013) and SSA (and its spectral variability) (*Sharma et al.*, 2013).

Key results for bare mineral dust aerosol include: i) a strong sensitivity of dust optical properties to shape (DDSCAT predicts at 550 nm an average difference between spheroids and prisms of about 20% for MEC and MSC, while of about 5% for the MAC); ii) a consistency between DDSCAT predicted and observed values of MAC, MSC and SSA reported by *Hand and Malm* (2007); and iii) a typical decrease in the SSA magnitude for wavelengths shorter than 500 nm (also found to be characteristic of organics and the aerosols mixture of Sodium Chloride and BC, see also *Scarnato et al.* (2013); *Russell et al.* (2010)).

Key results for polluted mineral dust, an internal mixture of BC and mineral dust, include: i) a strong decrease in MAC values with the increase in dust particle size (case BL2S1 presents largest values), while the opposite for SSA values. ii) A decrease in the SSA magnitude compared to bare dust for smaller dust particle sizes (cases BL2S1 and BL2S2) in agreement with *Clarke et al.* (2004). Further, iii) strong differences in predicted magnitude and spectral dependence of $C_{abs,scat,ext}$ when mixing a BC aggregate (case BL2) externally or internally with large mineral dust particles (cases S3, S5, BL2S3, BL2S5).

With this study, we demonstrated the importance of i) characterizing and defining micro-physical properties, such as morphology/shape and mixing of different aerosol types collected in ambient air, ii) estimating optical properties accordingly to observations, and iii) in defining eventual benchmarks errors due to use of approxima-

tions in shape and mixing. More studies are needed to assess the abundance of polluted dust particles in the atmosphere. In fact, the occurrence of such configuration is currently highly uncertain and might strongly depend on source and transport regions. Accounting for changes in optical properties induced by mixing as well as of the abundance of mixed particles, might be critical not only for calculating the relevance of such particles on regional radiative forcing, but also to understand biases in remote sensing techniques and to explore the potential of such techniques in remotely detecting mixed particles cases.

5 Acknowledgments

The work in this paper has been funded by the Research Initiation Program at the Naval Postgraduate school. Some of the work discussed in this paper was funded through the following grants: NASA (grant NNX13AN68H), NSF (grant AGS-1110059), DOE (grants DE-SC0006941 and DE-SC0010019). S. China and C. Mazzoleni would also like to acknowledge the contribution of several collaborators while collecting aerosol samples in several field campaigns and utilized here. Scarnato would like to acknowledge Dr. Denis Richard for providing aggregation code, Dr. Sanaz Vahidinia for building a first version of internal mixing code.

References

Adachi, K., and P. R. Buseck, Changes of ns-soot mixing states and shapes in an urban area during calnex, *Journal of Geophysical Research: Atmospheres*, pp. n/a–n/a, doi:10.1002/jgrd.50321, 2013.

Adachi, K., S. H. Chung, H. Friedrich, and P. R. Buseck, Fractal parameters of individual soot particles determined using electron tomography: Implications for optical properties, *Journal of Geophysical Research: Atmospheres*, *112*(D14), n/a–n/a, doi:10.1029/2006JD008296, 2007.

Adachi, K., S. Chung, and P. Buseck, Shapes of soot aerosol particles and implications for their effects on climate, *J. Geophys. Res.*, *115*(D15), doi:10.1029/2009JD012868, 2010.

Berry, M., and I. Percival, Optics of fractal clusters such as smoke, *Opt. Acta*, *33*, 1986.

Bond, T., and Bergstrom, Light Absorption by Carbonaceous Particles: An investigative Review, *Aerosol Sci. Tecnol.*, *40*, 27–67, 2006.

Bond, T. C., et al., Bounding the role of black carbon in the climate system: A scientific assessment, *Journal of Geophysical Research: Atmospheres*, *118*(11), 5380–5552, doi:10.1002/jgrd.50171, 2013.

Bueno, P. A., D. Havey, G. Mulholland, J. Hodges, K. Gillis, R. Dickerson, and M. Zachariah, Photoacoustic Measurements of Amplification of the Absorption Cross Section for Coated Soot Aerosols, *Aerosol Sci. Tecnol.*, *45*, 1217–1230, doi:10.1080/02786826.2011.587477, 2011.

Cappa, C., et al., Radiative absorption enhancements due to the mixing state of atmospheric black carbon, *Science*, *337*(6098), 1078–1081, doi:10.1126/science.1223447, 2012a.

Cappa, C. D., et al., Radiative absorption enhancements due to the mixing state of atmospheric black carbon, *Science*, *337*(6098), 1078–1081, 2012b.

Chang, H., and T. T. Charalampopoulos, Determination of the wavelength dependence of refractive indices of flame soot., *Proc. Roy. Soc. London*, *1*(430A), 577–591, 1990.

Chester, R., and et al., Eolian dust along the easter margins, *Mar. Geol.*, *13*(4), 91–106, 1972.

China, S., C. Mazzoleni, K. Gorkowski, A. C. Aiken, and M. K. Dubey, Morphology and mixing state of individual freshly emitted wildfire carbonaceous particles, *Nat Commun*, *4*, 2013.

China, S., N. Salvadori, and C. Mazzoleni, Effect of traffic and driving characteristics on morphology of atmospheric soot particles at freeway on-ramps, *Environmental Science and Technology*, *0*(0), null, doi:10.1021/es405178n, 2014.

China, S., et al., Morphology and mixing state of aged soot particles at a remote marine freetropospheric site: Implications to optical properties, *Accepted for publication- Geophysical Research Journal Letter*, 2015.

Chou, C., P. Formenti, M. Maille, P. Ausset, and G. Helas, Size distribution, shape, and composition of mineral dust aerosols collected during the African Monsoon Multidisciplinary Analysis Special Observation Period 0: dust and biomass-burning experiment field campaign in Niger, *J. Geophys. Res.*, *113*, doi:10.1029/2008JD009897, 2006.

Chylek, P., and J. Wong, Effect of absorbing aerosols on global radiation budget, *Geophysical Research Letters*, *22*(8), 929–931, doi:10.1029/95GL00800, 1995.

Clarke, A. D., et al., Size distributions and mixtures of dust and black carbon aerosol in Asian outflow: Physiochemistry and optical properties, *Journal of Geophysical Research: Atmospheres*, *109*(D15), n/a–n/a, doi:10.1029/2003JD004378, 2004.

Cross, E. S., et al., Soot particle studies—instrument inter-comparison—project overview, *Aerosol Sci. Tecnol.*, *44*(8), 592–611, doi:10.1080/02786826.2010.482113, 2010.

Deuze, J., et al., Remote sensing of aerosols over land surfaces from polder-adeos-1 polarized measurements, *J. Geophys. Res.*,

106, 4913–4926, doi:10.1029/2000JD900364, 2001.

Draine, B., and Flatau, Discrete dipole approximation for scattering calculations, *J. Opt. Soc. Am. A*, *11*, 1491–1499, 1994.

Draine, B., and Flatau, User Guide to the Discrete Dipole Approximation Code DDSCAT 7.1, *Cornell University Library*, 2010.

Dubovik, O., B. N. Holben, T. Lapyonok, A. Sinyuk, M. I. Mishchenko, P. Yang, and I. Slutsker, Non-spherical aerosol retrieval method employing light scattering by spheroids, *Geophysical Research Letters*, *29*(10), 541–544, doi:10.1029/2001GL014506, 2002.

Dubovik, O., A. Sinyuk, T. Lapyonok, and M. Holben, B. N. nd Mishchenko, Application of spheroid models to account for aerosol particle nonsphericity in remote sensing of desert dust, *J. Geophys. Res.*, *111*, doi:10.1029/2005JD006619, 2006.

Durkee, P. A., et al., Regional aerosol optical depth characteristics from satellite observations: ACE-1, TARFOX and ACE-2 results, *Tellus B*, *52*(2), 484 – 497, doi:10.1034/j.1600-0889.2000.00040.x, 2000.

Dzepina, K., et al., Molecular characterization of free tropospheric aerosol collected at the pico mountain observatory: a case study with long range transported biomass burning plumes, *Atmospheric Chemistry and Physics Discussions*, *14*(17), 24,753–24,810, doi:10.5194/acpd-14-24753-2014, 2014.

Fuller, K. A., W. C. Malm, and S. M. Kreidenweis, Effects of mixing on extinction by carbonaceous particles, *J. Geophys. Res.*, *104*, 15,941–15,954, 1999.

Gyawali, M., et al., Photoacoustic optical properties at uv, vis, and near ir wavelengths for laboratory generated and winter time ambient urban aerosols, *Atmospheric Chemistry and Physics*, *12*(5), 2587–2601, doi:10.5194/acp-12-2587-2012, 2012.

Hand, J. L., and W. C. Malm, Review of aerosol mass scattering efficiencies from ground-based measurements since 1990, *Journal of Geophysical Research: Atmospheres*, *112*(D16), n/a–n/a, doi:10.1029/2007JD008484, 2007.

Hansell Jr., R. A., J. S. Reid, S. C. Tsay, T. L. Roush, and O. V. Kalashnikova, A sensitivity study on the effects of particle chemistry, asphericity and size on the mass extinction efficiency of mineral dust in the earth's atmosphere: from the near to thermal ir, *Atmospheric Chemistry and Physics*, *11*(4), 1527–1547, doi:10.5194/acp-11-1527-2011, 2011.

Hasekamp, O., P. Litvinov, and A. Butz, Aerosol properties over the ocean from PARASOL multiangle photopolarimetric measurements, *J. Geophys. Res.*, *116*, doi:10.1029/2010JD015469, 2011.

Haywood, J. M., et al., Overview of the dust and biomass-burning experiment and african monsoon multidisciplinary analysis special observing period-0, *Journal of Geophysical Research: Atmospheres*, *113*(D23), n/a–n/a, doi:10.1029/2008JD010077, 2008.

Honrath, R., R. C. Owen, M. Val Martin, J. Reid, K. Lapina, P. Fialho, M. P. Dziobak, J. Kleissl, and D. Westphal, Regional and hemispheric impacts of anthropogenic and biomass burning emissions on summertime co and o_3 in the north atlantic lower free troposphere, *Journal of Geophysical Research: Atmospheres (1984-2012)*, *109*(D24), 2004.

Jacobson, M., Strong radiative heating due to mixing state of black carbon in atmospheric aerosol., *Letters to Nature*, pp. 695–697, 2001.

Jacobson, M. Z., Effects of biomass burning on climate, accounting for heat and moisture fluxes, black and brown carbon, and cloud absorption effects, *Journal of Geophysical Research: Atmospheres*, *119*(14), 8980–9002, doi:10.1002/2014JD021861, 2014.

Johnson, B. T., S. R. Osborne, J. M. Haywood, and M. A. J. Harrison, Aircraft measurements of biomass burning aerosol over west africa during dabex, *Journal of Geophysical Research: Atmospheres*, *113*(D23), n/a–n/a, doi:10.1029/2007JD009451, 2008.

Kahnert, M., On the discrepancy between modeled and measured mass absorption cross sections of light absorbing carbon

aerosols, *Aerosol Sci. Tecnol.*, *44*(6), 453–460, doi:10.1080/02786821003733834, 2010a.

Kahnert, M., Numerically exact computation of the optical properties of light absorbing carbon aggregates for wavelength of 200 nm to 12 microns, *Atmospheric Chemistry and Physics*, *10*(17), 8319–8329, doi:10.5194/acp-10-8319-2010, 2010b.

Kahnert, M., and A. Devasthale, Black carbon fractal morphology and short-wave radiative impact: a modelling study, *Atmospheric Chemistry and Physics*, *11*(22), 11,745–11,759, doi:10.5194/acp-11-11745-2011, 2011.

Kahnert, M., T. Nousiainen, H. Lindqvist, and M. Ebert, Optical properties of light absorbing carbon aggregates mixed with sulfate: assessment of different model geometries for climate forcing calculations, *Opt. Express*, *20*(9), 10,042–10,058, doi:10.1364/OE.20.010042, 2012.

Kalashnikova, O. V., M. J. Garay, J. V. Martonchik, and D. J. Diner, Misr dark water aerosol retrievals: operational algorithm sensitivity to particle non-sphericity, *Atmospheric Measurement Techniques*, *6*(8), 2131–2154, doi:10.5194/amt-6-2131-2013, 2013.

Kandler, K., L. Schutz, C. Deutscher, M. Ebert, and H. Hofmann, Size distribution, mass concentration, chemical and mineralogical composition, and derived optical parameters of the boundary layer aerosol at tinfou, morocco, during SAMUM, *Tellus*, *61B*, 2006.

Kim, D., C. Wang, A. M. L. Ekman, M. C. Barth, and P. J. Rasch, Distribution and direct radiative forcing of carbonaceous and sulfate aerosols in an interactive size-resolving aerosolclimate model, *Journal of Geophysical Research: Atmospheres*, *113*(D16), n/a–n/a, doi:10.1029/2007JD009756, d16309, 2008.

Klingmüller, K., B. Steil, C. Brühl, H. Tost, and J. Lelieveld, Sensitivity of aerosol radiative effects to different mixing assumptions in the aeropt 1.0 submodel of the emac atmospheric-chemistryclimate model, *Geoscientific Model Development*, *7*(5), 2503–2516, doi:10.5194/gmd-7-2503-2014, 2014.

Koch, D., et al., Evaluation of black carbon estimations in global aerosol models, *Atmospheric Chemistry and Physics*, *9*(22), 9001–9026, doi:10.5194/acp-9-9001-2009, 2009.

Lack, D. A., and J. M. Langridge, On the attribution of black and brown carbon light absorption using the ångstrom exponent, *Atmospheric Chemistry and Physics Discussions*, *13*(6), 15,493–15,515, doi:10.5194/acpd-13-15493-2013, 2013.

Lau, K., and K. Kim, Observational relationships between aerosol and asian monsoon rainfall, and circulation, *Geophysical Research Letters*, *33*(21), n/a–n/a, doi:10.1029/2006GL027546, 2006.

Liu, L., M. M.I., and A. W.P., A study of radiative properties of fractal soot aggregates using the superposition T-matrix method, *J. Quant. Spec. Rad. Transfer.*, *109*, 2656–663, 2008.

McConnell, C. L., P. Formenti, E. J. Highwood, and M. A. J. Harrison, Using aircraft measurements to determine the refractive index of Saharan dust during the DODO Experiments, *Atmospheric Chemistry and Physics*, *10*(6), 3081–3098, doi:10.5194/acp-10-3081-2010, 2010.

Merikallio, S., H. Lindqvist, T. Nousiainen, and M. Kahnert, Modelling light scattering by mineral dust using spheroids: assessment of applicability, *Atmospheric Chemistry and Physics Discussions*, *11*(2), 3977–4016, doi:10.5194/acpd-11-3977-2011, 2011.

Mishra, S. K., S. N. Tripathi, S. Aggarwal, and A. Arola, Optical properties of accumulation mode, polluted mineral dust: effects of particle shape, hematite content and semi-external mixing with carbonaceous species, *Tellus B*, *64*(0), 2012.

Moosmueller, H., W. P. Arnott, C. F. Rogers, J. C. Chow, C. A. Frazier, L. E. Sherman, and D. L. Dietrich, Photoacoustic and filter measurements related to aerosol light absorption during the northern front range air quality study (*c*olorado 1996/1997), *Journal of Geophysical Research: Atmospheres*, *103*(D21), 28,149–28,157, doi:10.1029/98JD02618, 1998.

Nousiainen, T., Optical modeling of mineral dust particles: A review, *Journal of Quantitative Spectroscopy and Radiative*

Transfer, *110*(14), 1261–1279, 2009.

Oh, C., and C. Sorensen, The effect of overlap between monomers on the determination of fractal cluster morphology, *Journal of Colloid and Interface Science*, *193*(1), 17 – 25, doi:http://dx.doi.org/10.1006/jcis.1997.5046, 1997.

Osborne, S. R., B. T. Johnson, J. M. Haywood, A. J. Baran, M. A. J. Harrison, and C. L. McConnell, Physical and optical properties of mineral dust aerosol during the dust and biomass-burning experiment, *Journal of Geophysical Research: Atmospheres*, *113*(D23), n/a–n/a, doi:10.1029/2007JD009551, 2008.

Otto, S., T. Trautmann, and M. Wendisch, On realistic size equivalence and shape of spheroidal saharan mineral dust particles applied in solar and thermal radiative transfer calculations, *Atmospheric Chemistry and Physics*, *11*(9), 4469–4490, doi:10.5194/acp-11-4469-2011, 2011.

Prospero, J. M., R. A. Glaccum, and R. T. Nees, Atmospheric transport of soil dust from africa to south america, *Nature*, *289*, 1981.

Reale, O., K. M. Lau, and A. da Silva, Impact of interactive aerosol on the african easterly jet in the nasa geos-5 global forecasting system., *Wea. Forecasting*, pp. 504–519, doi:http://dx.doi.org/10.1175/WAF-D-10-05025.1, 2011.

Reid, E. A., J. S. Reid, M. M. Meier, M. R. Dunlap, and S. S. Cliff, Characterization of african dust transported to puerto rico by individual particle and size segregated bulk analysis, *J. Geophys. Res.*, *108(D19)*, doi:10.1029/2002JD002935, 2003.

Richard, D., D. Glenar, T. Stubbs, S. Davis, and A. Colaprete, Light scattering by complex particles in the moon's exosphere: Toward a taxonomy of models for the realistic simulation of the scattering behavior of lunar dust, *Planetary and Space Science*, *59*(14), 1804 – 1814, doi:http://dx.doi.org/10.1016/j.pss.2011.01.003, lunar Dust, Atmosphere and Plasma: The Next Steps, 2011.

Richard, D. T., and S. S. Davis, Lunar dust characterization by polarimetric signature, *AA*, *483*(2), 643–649, doi:10.1051/0004-6361:20079108, 2008.

Russell, P., and J. Heintzenburg, An overview of the ACE-2 clear sky column closure experiment, *Tellus*, *52*, 463–483, 2000.

Russell, P., et al., Absorption Angstrom Exponent in AERONET and related data as an indicator of aerosol composition, *Atmos. Chem. Phys.*, *10*, 1155–1169, 2010.

Ryder, C. L., et al., Optical properties of saharan dust aerosol and contribution from the coarse mode as measured during the fennec 2011 aircraft campaign, *Atmospheric Chemistry and Physics*, *13*(1), 303–325, doi:10.5194/acp-13-303-2013, 2013.

Samset, B. H., et al., Black carbon vertical profiles strongly affect its radiative forcing uncertainty, *Atmospheric Chemistry and Physics*, *13*(5), 2423–2434, doi:10.5194/acp-13-2423-2013, 2013.

Samson, R. J., G. W. Mulholland, and J. W. Gentry, Structural analysis of soot agglomerates, *Langmuir*, *3*(2), 272–281, doi:10.1021/la00074a022, 1987.

Scarnato, B. V., S. Vahidinia, D. T. Richard, and T. W. Kirchstetter, Effects of internal mixing and aggregate morphology on optical properties of black carbon using a discrete dipole approximation model, *Atmospheric Chemistry and Physics*, *13*(10), 5089–5101, doi:10.5194/acp-13-5089-2013, 2013.

Sharma, N., I. J. Arnold, H. Moosmueller, W. P. Arnott, and C. Mazzoleni, Photoacoustic and nephelometric spectroscopy of aerosol optical properties with a supercontinuum light source, *Atmospheric Measurement Techniques*, *6*(12), 3501–3513, doi:10.5194/amt-6-3501-2013, 2013.

Shen, Y., B. T. Draine, and T. J. Eric, Modeling Porous Dust Grains with Ballistic Aggregates. i. Geometry and Optical Properties, *The Astrophysical Journal*, *689*(1), 260, 2008.

Sokolik, I. N., and O. B. Toon, Incorporation of mineralogical composition into models of the radiative properties of mineral aerosol from uv to ir wavelengths, *Journal of Geophysical Research: Atmospheres*, *104*(D8), 9423–9444, doi:10.1029/

1998JD200048, 1999.

Sokolik, I. N., D. M. Winker, G. Bergametti, D. A. Gillette, G. Carmichael, Y. J. Kaufman, L. Gomes, L. Schuetz, and J. E. Penner, Introduction to special section: Outstanding problems in quantifying the radiative impacts of mineral dust, *Journal of Geophysical Research: Atmospheres*, *106*(D16), 18,015–18,027, doi:10.1029/2000JD900498, 2001.

Tanre, D., et al., Measurement and modeling of the Saharan dust radiative impact: Overview of the Saharan Dust Experiment (SHADE), *Journal of Geophysical Research: Atmospheres*, *108*(D18), doi:10.1029/2002JD003273, 2003.

Usher, C. R., A. E. Michel, and V. H. Grassian, Reactions on mineral dust, *Chemical Reviews*, *103*(12), 4883–4940, doi:10.1021/cr020657y, 2003.

Wagner, R., T. Ajtai, K. Kandler, K. Lieke, C. Linke, T. Mueller, M. Schnaiter, and M. Vragel, Complex refractive indices of saharan dust samples at visible and near uv wavelengths: a laboratory study, *Atmospheric Chemistry and Physics*, *12*(5), 2491–2512, doi:10.5194/acp-12-2491-2012, 2012.

Xue, H., A. F. Khalizov, L. Wang, J. Zheng, and R. Zhang, Effects of dicarboxylic acid coating on the optical properties of soot, *Chem. Chem. Phys.*, *11*, 7869–7875, doi:10.1039/B904129J, 2009.

Yoshida, M., J. M. Haywood, T. Yokohata, H. Murakami, and T. Nakajima, Spatial distribution of dust's optical properties over the sahara and asia inferred from moderate resolution imaging spectroradiometer, *Atmospheric Chemistry and Physics*, *13*(21), 10,827–10,845, doi:10.5194/acp-13-10827-2013, 2013.

Zaveri, R. A., et al., Overview of the 2010 carbonaceous aerosols and radiative effects study (cares), *Atmospheric Chemistry and Physics*, *12*(16), 7647–7687, doi:10.5194/acp-12-7647-2012, 2012.

Zhang, R., A. F. Khalizov, J. Pagels, D. Zhang, H. Xue, and P. H. McMurry, Variability in morphology, hygroscopicity, and optical properties of soot aerosols during atmospheric processing, *Proceedings of the National Academy of Sciences*, *105*(30), 10,291–10,296, doi:10.1073/pnas.0804860105, 2008.